Mesoporous Materials

Deutsche Ausgabe: DOI: 10.1002/ange.201501398
Internationale Ausgabe: DOI: 10.1002/anie.201501398

Highly Ordered Mesoporous Few-Layer Graphene Frameworks Enabled by Fe_3O_4 Nanocrystal Superlattices**

*Yucong Jiao, Dandan Han, Limin Liu, Li Ji, Guannan Guo, Jianhua Hu, Dong Yang, and Angang Dong**

Abstract: *While great progress has been achieved in the synthesis of ordered mesoporous carbons in the past decade, it still remains a challenge to prepare highly graphitic frameworks with ordered mesoporosity and high surface area. Reported herein is a simple synthetic methodology, based on the conversion of self-assembled superlattices of Fe_3O_4 nanocrystals, to fabricate highly ordered mesoporous graphene frameworks (MGFs) with ultrathin pore walls consisting of three to six stacking graphene layers. The MGFs possess face-centered-cubic symmetry with interconnected mesoporosity, tunable pore width, and high surface area. Because of their unique architectures and superior structural durability, the MGFs exhibit excellent cycling stability and rate performance when used as anode materials for lithium-ion batteries, thus retaining a specific capacity of 520 mAh g^{-1} at a current density of 300 mA g^{-1} after 400 cycles.*

Nanostructured carbons,[1–8] including carbon nanotubes,[2] graphene,[3] and porous carbons,[4–8] represent an innovative class of technologically important materials. In particular, ordered mesoporous carbons (OMCs) with pore sizes tunable in the range of 2–50 nm have attracted increasingly greater attention because of their ordered mesoporosity, high surface area, and adjustable pore symmetry,[5] which have found wide applications in energy storage devices such as lithium-ion batteries (LIBs) and supercapacitors.[1a] Current methods of preparing OMCs rely on a templating strategy.[5] Both mesoporous silica and silica opals have been widely employed as hard templates to prepare OMCs through a nanocasting mechanism.[6,7] More recently, block co-polymers have been used as a soft template for the direct synthesis of OMCs,[8] in analogy to the preparation of ordered mesoporous silica.[9]

In spite of the aforementioned synthetic progress, most OMCs obtained to date are amorphous in nature,[6–8] and it may limit their applications, as the physicochemical properties (electronic conductivity and chemical stability, etc.) of porous carbon materials strongly depend on the crystallinity (i.e., graphitization degree) of the pore walls.[10] Highly graphitic porous carbons are attainable by heating the preformed OMCs at high temperatures (> 2500 °C),[11] which unfortunately can lead to the loss of surface area and structural ordering arising from pore collapse. Graphitic mesoporous carbons can also be realized at relatively low temperatures (< 1500 °C) by introducing metals or metal oxides as graphitization catalysts.[12] Despite the possibility to preserve the structural ordering by using this strategy, the resulting carbon frameworks are usually partially graphitic or semigraphitic as a result of the low graphitization temperature. Therefore, it still remains a challenge to synthesize highly graphitic frameworks with well-defined mesoporosity and high surface area.[13]

Herein, we report a strategy of preparing highly ordered mesoporous graphene frameworks (MGFs) with pore walls consisting of three to six stacking graphene layers. As illustrated in Scheme 1, three-dimensional (3D) superlattices self-assembled from colloidal Fe_3O_4 nanocrystals (NCs) capped with oleic acid (OA) are first used to produce

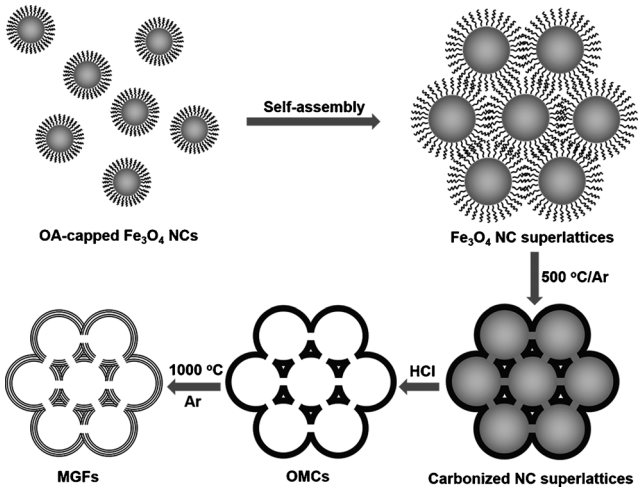

Scheme 1. Schematic illustration of the fabrication of MGFs from colloidal Fe_3O_4 NCs (cross-sectional view).

[*] Y. Jiao, D. Han, L. Ji, Prof. A. Dong
Collaborative Innovation Center of Chemistry for Energy Materials
Shanghai Key Laboratory of Molecular Catalysis and Innovative Materials, and Department of Chemistry
Fudan University, Shanghai 200433 (China)
E-mail: agdong@fudan.edu.cn
L. Liu, G. Guo, Prof. J. Hu, Prof. D. Yang
State Key Laboratory of Molecular Engineering of Polymers
Collaborative Innovation Center of Polymers and Polymer Composite Materials, and Department of Macromolecular Science
Fudan University, Shanghai 200433 (China)

[**] D.Y. is grateful for financial support from the Natural National Science Foundation of China (51103026, 51373035, and 51373040), the Shanghai Scientific and Technological Innovation Project (11JC1400600 and 124119a2400), and International Science & Technology Cooperation Program of China (2014DFE40130). A.D. acknowledges financial support from Fudan University, the "1000 Youth Talents" Plan, Natural National Science Foundation of China (21373052), and the National Basic Research Program of China (973 program: 2014CB845602).

Supporting information for this article is available on the WWW under http://dx.doi.org/10.1002/anie.201501398.

OMCs upon the carbonization of OA ligands followed by the removal of Fe_3O_4 NCs. The Fe_3O_4-NC-derived OMCs are then converted into MGFs by simple heat treatment at 1000 °C in argon. The resulting MGFs are characterized by highly ordered and interconnected mesoporosity, large pore volume (ca. 1.8 $cm^3 g^{-1}$), and high surface area (ca. 1000 $m^2 g^{-1}$), with the pore width tunable to within the range of 8–20 nm by controlling that of Fe_3O_4 NCs. When evaluated as LIB anode materials, MGFs exhibit outstanding cycling performance and rate capability, which are attributable to their unique architectures and superior structural durability.

Figure 1a shows a typical high-resolution scanning electron microscopy (HRSEM) image of 12 nm Fe_3O_4 NC superlattices, which are obtained by drying of an NC solution in *n*-hexane under ambient conditions.[14] The long-range NC ordering is attributed to the high monodispersity of Fe_3O_4 NCs used for self-assembly,[14a] and accounts for the highly ordered porous structure of the subsequently formed OMCs and MGFs. The as-assembled Fe_3O_4 NC superlattices typically adopt face-centered-cubic (fcc) symmetry as indicated by small-angle X-ray scattering (SAXS; see Figure S1 in the Supporting Information). To carbonize the surface-coating OA ligands, the as-assembled Fe_3O_4 NC superlattices are subject to heat treatment at 500 °C in argon for 2 hours, which proves to be optimal conditions for enabling ligand carbonization without disrupting the ordered structure of NC superlattices (see Figure S2). Highly ordered mesoporous carbon frameworks are obtained upon the removal of Fe_3O_4 NCs by acid etching. As unambiguously confirmed by transmission electron microscopy (TEM, Figure 1b), SAXS (see Figure S3), and N_2 adsorption-desorption measurements (see Figure S4), the resulting OMCs possess the same fcc symmetry as Fe_3O_4 NC superlattices, with pore walls composed of interconnected ultrathin carbon shells (ca. 2 nm) resulting from ligand carbonization.

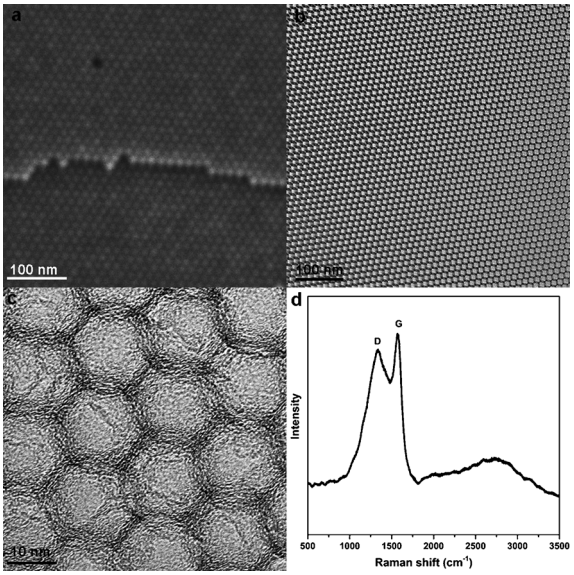

Figure 1. a) Representative HRSEM image of Fe_3O_4 NC superlattices. b,c) TEM and HRTEM images Fe_3O_4-NC-derived OMCs, respectively. d) Representative Raman spectrum of Fe_3O_4-NC-derived OMCs.

It is noteworthy that our method to prepare OMCs differs significantly from previous templating approaches in that the Fe_3O_4 NCs employed serve as not only template but also as a graphitization catalyst, thus rendering OMCs with partially graphitic pore walls, as evidenced by high-resolution TEM (HRTEM, Figure 1c) and Raman spectroscopy (Figure 1d). Remarkably, such partially graphitic, ultrathin pore walls can be readily converted into stacking graphene layers by heat treatment at temperatures as low as 1000 °C (see Figure S5), thus resulting in MGFs with well-maintained structural ordering as indicated by low-magnification TEM images and fast Fourier transforms (FFTs; see Figure 2a,b and Figure S6). HRTEM reveals that the pore walls of MGFs are composed of three to six stacking graphene layers depending on the thickness (Figure 2c,d), with an interlayer spacing of about 0.355 nm (see Figure S7), which is close to the typical value for graphite (0.335 nm).[15] Interestingly, all the graphene layers display a circle-like curvature apparently derived from the spherical Fe_3O_4 NCs, thus implying Fe_3O_4

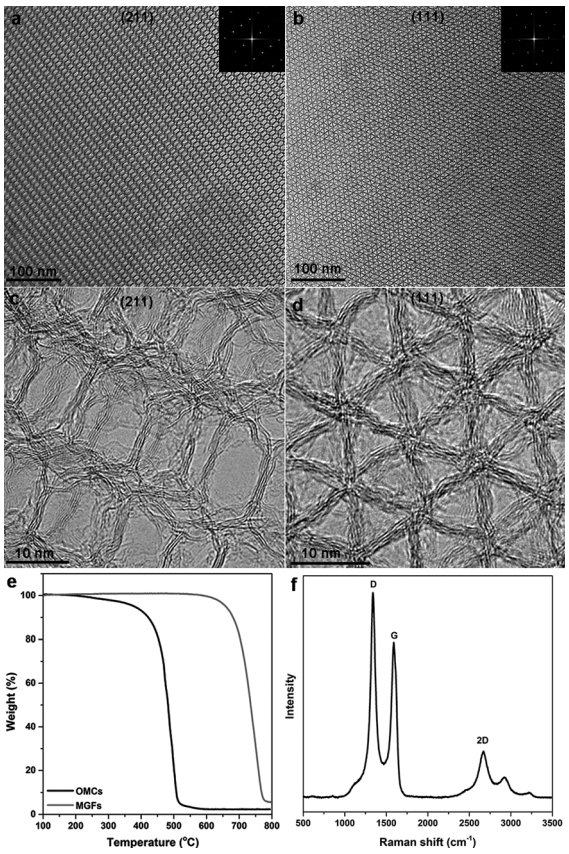

Figure 2. a,b) Low-magnification TEM images and the corresponding FFTs (inset) of MGFs along the (211) and (111) directions, respectively. c,d) HRTEM images of MGFs along the (211) and (111) directions, respectively. e) TGA curves of OMCs and their derived MGFs, which are acquired in air with a heating rate of 10 °C min^{-1}. The residual mass in both cases is presumably attributed to the small fraction of unremoved Fe_3O_4 NCs. f) Representative Raman spectrum of MGFs.

NCs indeed play a catalytic role during the carbon framework formation.

Thermogravimetric analysis (TGA) carried out in air indicates that the carbon combustion temperature of MGFs is about 750 °C, which is much higher than that (ca. 490 °C) of OMCs (Figure 2e). This study provides further evidence of the well-crystallized nature of MGFs, as graphitic carbons have been reported to be more stable against oxidation than amorphous carbons because of the improved crystallinity.[12a] The TGA residue (ca. 2–5 wt%) in both cases is presumably caused by the small amount of unremoved Fe_3O_4 NCs during acid etching, and could, in principle, be completely etched away by increasing the etching time. Wide-angle X-ray scattering (XRD) is also used to evaluate the crystallinity of MGFs (see Figure S8). The wide (002) peak at about 25° indicates that the crystallinity of MGFs is lower than that of graphite, and could be attributed to the curvature as well as the ultrathin thickness of the graphitic shells.[16a] The graphitization degree of MGFs is further characterized using Raman spectroscopy. The well-resolved G and 2D bands at 1588 and 2671 cm^{-1}, respectively, suggest the highly graphitic nature of the pore walls (Figure 2f).[16] The intensity ratio of the 2D and G bands (I_{2D}/I_G) is equal to 0.65, and indicative of a multilayer graphene structure consistent with HRTEM observations.[16c,d] Although significantly improved upon graphitization, we note that the graphitization degree of MGFs is inferior to that of perfect graphene or few-layer graphene layers fabricated by chemical vapor deposition (CVD),[16d,e] as indicated by the strong disorder-induced D band. This band is probably caused by structural defects introduced during the etching and/or graphitization processes. Nonetheless, TEM, TGA, XRD, and Raman spectroscopy establish that heat treatment at 1000 °C successfully converts the pore walls of OMCs into few-layer graphene without disrupting the ordered porous structure.

Having established the highly graphitic nature of MGFs, we turned our attention to their detailed structural and textural properties. Figure 3a shows a typical SAXS pattern of MGFs, and exhibits at least nine well-resolved scattering peaks indexed to a highly ordered fcc structure inherited from Fe_3O_4 NC superlattices, thus further confirming that the graphitization process does not affect the symmetry and structural ordering of OMCs, and is consistent with the TEM results. Figure 3b presents the SAXS patterns of a series of MGFs with different pore widths ranging from 9 to 16 nm, which are obtained by varying the diameter of the original Fe_3O_4 NCs used for superlattice formation. Despite different pore widths, all the MGF samples exhibit a long-range ordered fcc structure as indicated by the sharp scattering peaks, thus suggesting that the variation of NC size does not affect the symmetry and structural ordering of the resulting MGFs. Figure 3c shows typical N_2 adsorption–desorption curves of MGFs derived from 12 nm Fe_3O_4 NCs, which exhibit prominent characteristics of type-IV isotherms, while the large H_2-type hysteresis loop at P/P_0 of about 0.47 implies a caged mesoporous structure with small openings on the pore walls,[17] similar to the case of OMCs (Figure S4). The pore width distribution curve indicates that the interconnected openings are about 3 nm in dimension (Figure 3d). These

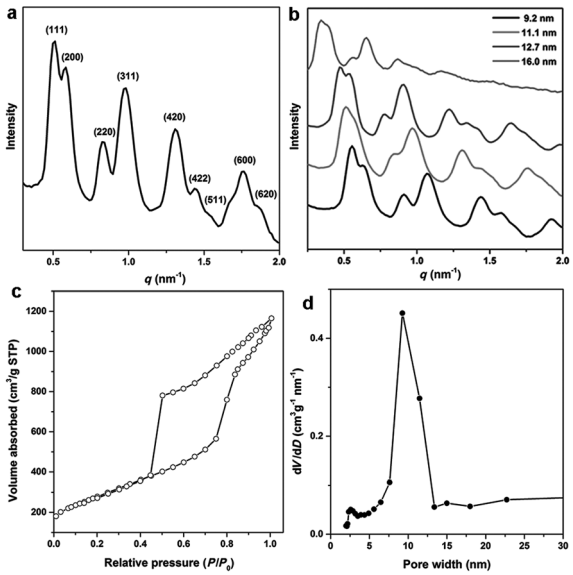

Figure 3. a) Representative SAXS pattern of MGFs derived from 12 nm Fe_3O_4 NC superlattices. b) SAXS pattern of a series of MGFs with different pore widths. c,d) N_2 adsorption-desorption isotherms and pore width distribution of MGFs derived from 12 nm Fe_3O_4 NC superlattices, respectively.

results suggest that the ultrathin pore walls of MGFs are interconnected to form a 3D continuous porous structure. The typical Brunauer–Emmett–Teller (BET) surface area of MGFs is about 1000 $m^2 g^{-1}$ with a pore volume of approximately 1.8 $cm^3 g^{-1}$. Notably, the BET surface area of MGFs is higher than that of many ordered graphitic mesoporous carbons reported previously.[18]

Because of their highly ordered and accessible mesopores, large surface area, and high electronic conductivity, the MGFs obtained are expected to be particularly suitable as anode materials for LIBs. The electrochemical performance of MGF anodes is evaluated by both cyclic voltammetry and galvanostatic charge-discharge cycling. Cyclic voltammograms (CVs) of MGFs are conducted within the range from 3.0 to 0.005 V (vs. Li/Li^+) at a scan rate of 0.2 $mV s^{-1}$. As shown in Figure 4a, the CV curves of MGFs are consistent with those of many other carbon-based anode materials reported previously,[13c,19] and the prominent peak at about 0.55 V in the first cathodic sweep is primarily caused by the decomposition of electrolytes and the formation of solid electrolyte interphase (SEI).[13c] The CV curves almost overlap from the second cycle, and is indicative of the formation of a stable SEI layer. In the galvanostatic charge-discharge measurements at a current density of 300 $mA g^{-1}$, the MGF anode delivers a capacity of 2338 and 660 $mAh g^{-1}$ in the first discharge and charge processes, respectively (see Figure S9). The large initial capacity loss, which has been observed for many mesoporous carbon or graphene-based anodes,[19–23] is attributed to the enhanced SEI formation resulting from the large surface area of MGFs. Additionally, the presence of structural defects in MGFs can lead to irreversible Li insertion into frameworks, and may also contribute to the first-cycle capacity loss. Despite the first-cycle capacity loss, the charge-discharge

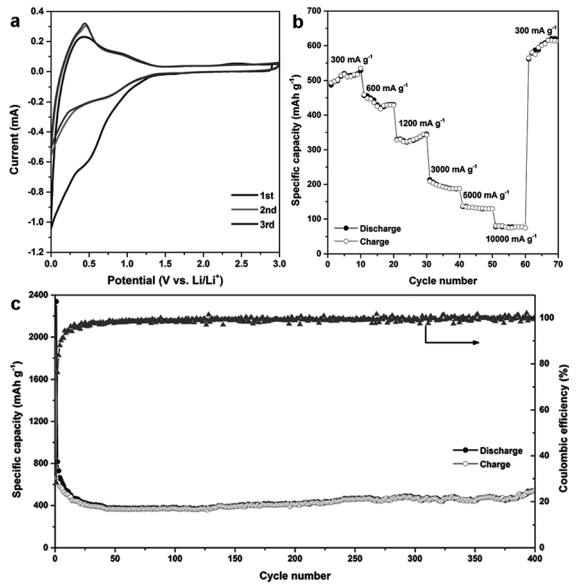

Figure 4. a) Representative CV curves of MGFs. b) Rate capability of MGFs tested at current densities ranging from 300 to 10000 mA g^{-1}. c) Cycling performance of MGFs at a current density of 300 mA g^{-1} and the corresponding Coulombic efficiency.

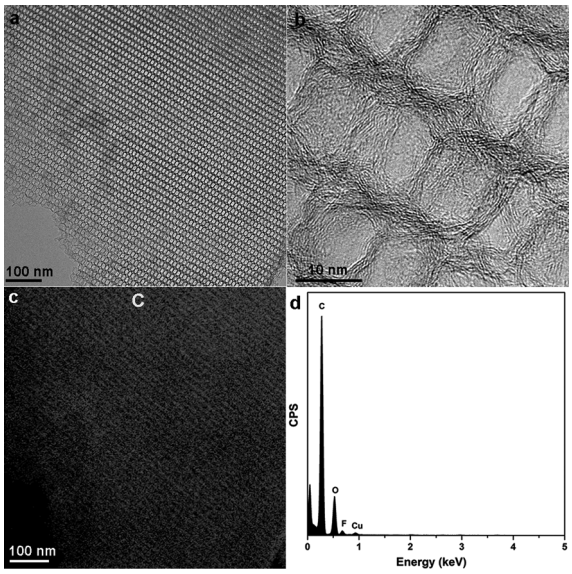

Figure 5. a,b) Low-magnification TEM and HRTEM images of MGFs after 400 cycles, respectively. c,d) Elemental mapping and EDS spectrum of the same MGFs as shown in (a), respectively. The F signal in (d) is attributed to the PVDF binder.

curves for the 50th and 200th cycles almost overlap with each other, thus implying good cycling stability. The rate capability is evaluated at different current densities ranging from 300 to 10000 mA g^{-1}. As shown in Figure 4b, the MGF anode is able to deliver reversible capacities of 432, 330, and 186 mAh g^{-1} at current densities of 600, 1200, and 3000 mA g^{-1}, respectively, and can still maintain reversible capacities of 127 and 80 mAh g^{-1} even at ultrahigh current densities of 5000 and 10000 mA g^{-1}, respectively. Furthermore, a high reversible capacity over 620 mAh g^{-1} is recovered when the current density is switched back to 300 mA g^{-1}. In addition to the excellent rate capability, our MGF anodes exhibit outstanding cycling performance. After continuous cycling for 400 cycles at a current density of 300 mA g^{-1}, the MGF anode can still maintain a specific capacity of 520 mAh g^{-1} (Figure 4c), which is much higher than the theoretical capacity for graphite (ca. 372 mAh g^{-1}). The lithium-storage properties of MGFs achieved in this work are superior to those of many state-of-the-art carbonaceous materials reported previously, including graphene sheets,[3b] interconnected hollow graphitic spheres,[20] graphene-constructed hollow spheres,[21] hierarchical porous carbons,[22] and carbon nanocages.[23]

We attribute the excellent electrochemical performance of MGFs to their unique architectures. Specifically, the 3D interconnected, ordered mesoporosity in combination with the large surface area of MGFs increases the contact area between the electrode and electrolyte, thus facilitating the access of Li ions into the electrode. In addition, the ultrathin pore walls greatly reduce the barriers for Li intercalation and extraction, which is beneficial for improving the rate performance. Furthermore, the continuous, highly graphitic frameworks can promote electron transport, which is also favorable for enhanced lithium-storage properties. To explore the structural evolution of MGFs during electrochemical reactions with Li, ex situ TEM and energy-dispersive X-ray spectroscopy (EDS) are performed on an MGF anode which has been cycled for 400 cycles at a current density of 300 mA g^{-1}. TEM indicates that both the structural ordering and the graphitic nature of MGFs are well preserved upon cycling (Figure 5a,b), thus suggesting that our MGFs possess exceptional structural stability and integrity, while elemental mapping and EDS confirm that the graphene frameworks are mainly composed of carbon, with a small fraction of F from the polyvinylidene fluoride (PVDF) binder (Figure 5c,d). The superior structural durability of MGFs also helps to explain their excellent cycling stability and rate performance.

In conclusion, our studies have established a robust and low-temperature synthetic methodology which employs self-assembled Fe_3O_4 NC superlattices to prepare 3D ordered mesoporous frameworks consisting of three to six stacking graphene layers. The successful formation of highly graphitic frameworks is attributed to the catalytic activity of Fe_3O_4 NCs as well as the ultrathin thickness of the pore walls. The MGFs obtained possess fcc symmetry with interconnected mesoporosity, tunable pore width, and high surface area. Because of their unique architecture and exceptional structural durability, MGFs exhibit excellent cycling performance and rate capability when evaluated as anode materials for LIBs, and retain a specific capacity of 520 mAh g^{-1} at a current density of 300 mA g^{-1} after 400 cycles. Although only Fe_3O_4 NCs are demonstrated for the preparation of MGFs in the current study, we anticipate that this novel synthetic concept can be readily extended to superlattices consisting of multicomponent NCs such as core/shell NCs and binary NCs.[24] This new approach will open new opportunities for the rational design of few-layer-graphene-based porous materials with more complicated architectures, which may find applications in catalysis, absorption, and energy storage.

Experimental Section

Self-assembly of Fe_3O_4 NC superlattices: Monodisperse, OA-stabilized Fe_3O_4 NCs with tunable sizes were synthesized and purified according to the literature method,[14a] and were dispersed in *n*-hexane to form a stable colloidal solution with a concentration of about 20 mg mL^{-1}. 3D superlattices of Fe_3O_4 NCs were fabricated by drying a colloidal solution of Fe_3O_4 NCs under ambient conditions.[14b]

Fabrication of MGFs: The as-assembled Fe_3O_4 NC superlattices were heated at 500 °C in argon for 2 h, carbonizing the surface-coating OA ligands. The carbonized Fe_3O_4 NC superlattices were refluxed in 10 M HCl, thus yielding OMCs upon the complete removal of Fe_3O_4 NCs. The as-synthesized OMCs were then subject to heat treatment at 1000 °C in argon for 2 h and resulted in MGFs while retaining structure ordering.

Keywords: graphene · lithium · mesoporous materials · nanostructures · self-assembly

How to cite: *Angew. Chem. Int. Ed.* **2015**, *54*, 5727–5731
Angew. Chem. **2015**, *127*, 5819–5823

[1] a) H. Nishihara, T. Kyotani, *Adv. Mater.* **2012**, *24*, 4473; b) S. Guo, S. Dong, *Chem. Soc. Rev.* **2011**, *40*, 2644; c) L. Zhang, X. Zhao, *Chem. Soc. Rev.* **2009**, *38*, 2520.

[2] a) R. H. Baughman, A. A. Zakhidov, W. A. de Heer, *Science* **2002**, *297*, 787; b) S. Iijima, T. Ichihashi, *Nature* **1993**, *363*, 603; c) A. C. Dillon, K. M. Jones, T. A. Bekkedahl, C. H. Kiang, D. S. Bethune, M. J. Heben, *Nature* **1997**, *386*, 377.

[3] a) A. K. Geim, K. S. Novoselov, *Nat. Mater.* **2007**, *6*, 183; b) E. Yoo, J. Kim, E. Hosono, H. Zhou, T. Kudo, I. Honma, *Nano Lett.* **2008**, *8*, 2277; c) T. Ohta, A. Bostwick, T. Seyller, K. Horn, E. Rotenberg, *Science* **2006**, *313*, 951.

[4] a) K. P. Gierszal, M. Jaroniec, *J. Am. Chem. Soc.* **2006**, *128*, 10026; b) B. Fang, M. Kim, J. H. Kim, S. Lim, J. Yu, *J. Mater. Chem.* **2010**, *20*, 10253; c) Z. Sun, Y. Liu, B. Li, J. Wei, M. Wang, Q. Yue, Y. Deng, S. Kaliaguine, D. Zhao, *ACS Nano* **2013**, *7*, 8706.

[5] a) R. Ryoo, S. H. Joo, M. Kruk, M. Jaroniec, *Adv. Mater.* **2001**, *13*, 677; b) C. Liang, Z. Li, S. Dai, *Angew. Chem. Int. Ed.* **2008**, *47*, 3696; *Angew. Chem.* **2008**, *120*, 3754.

[6] a) S. Jun, S. H. Joo, R. Ryoo, M. Kruk, M. Jaroniec, Z. Liu, T. Ohsuna, O. Terasaki, *J. Am. Chem. Soc.* **2000**, *122*, 10712; b) S. H. Joo, S. J. Choi, I. Oh, J. Kwak, Z. Liu, O. Terasaki, R. Ryoo, *Nature* **2001**, *412*, 169; c) J. Lee, K. Sohn, T. Hyeon, *J. Am. Chem. Soc.* **2001**, *123*, 5146.

[7] a) K. A. Cychosz, X. Guo, W. Fan, R. Cimino, G. Y. Gor, M. Tsapatsis, A. V. Neimark, M. Thommes, *Langmuir* **2012**, *28*, 12647; b) A. Vu, X. Li, J. Phillips, A. Han, W. H. Smyrl, P. Buehlmann, A. Stein, *Chem. Mater.* **2013**, *25*, 4137.

[8] a) T. Ma, L. Liu, Z. Yuan, *Chem. Soc. Rev.* **2013**, *42*, 3977; b) C. Liang, K. Hong, G. Guiochon, J. W. Mays, S. Dai, *Angew. Chem. Int. Ed.* **2004**, *43*, 5785; *Angew. Chem.* **2004**, *116*, 5909; c) Y. Meng, D. Gu, F. Zhang, Y. Shi, H. Yang, Z. Li, C. Yu, B. Tu, D. Zhao, *Angew. Chem. Int. Ed.* **2005**, *44*, 7053; *Angew. Chem.* **2005**, *117*, 7215.

[9] C. T. Kresge, M. E. Leonowicz, W. J. Roth, J. C. Vartuli, J. S. Beck, *Nature* **1992**, *359*, 710.

[10] a) Y. Xia, R. Mokaya, *Adv. Mater.* **2004**, *16*, 1553; b) F. Goettmann, A. Thomas, M. Antonietti, *Angew. Chem. Int. Ed.* **2007**, *46*, 2717; *Angew. Chem.* **2007**, *119*, 2773; c) H. Jiang, L. Yang, C. Li, C. Yan, P. S. Lee, J. Ma, *Energy Environ. Sci.* **2011**, *4*, 1813.

[11] a) A. B. Fuertes, S. Alvarez, *Carbon* **2004**, *42*, 3049; b) S. B. Yoon, G. S. Chai, S. K. Kang, J. Yu, K. P. Gierszal, M. Jaroniec, *J. Am. Chem. Soc.* **2005**, *127*, 4188.

[12] a) T. W. Kim, I. S. Park, R. Ryoo, *Angew. Chem. Int. Ed.* **2003**, *42*, 4375; *Angew. Chem.* **2003**, *115*, 4511; b) K. T. Lee, X. Ji, M. Rault, L. F. Nazar, *Angew. Chem. Int. Ed.* **2009**, *48*, 5661; *Angew. Chem.* **2009**, *121*, 5771; c) A. Wang, J. Ren, B. Shi, G. Lu, Y. Wang, *Microporous Mesoporous Mater.* **2012**, *151*, 287; d) A. Kong, Y. Kong, X. Zhu, Z. Han, Y. Shan, *Carbon* **2014**, *78*, 49; e) L. Zhang, W. Li, Z. Cui, W. Song, *J. Phys. Chem. C* **2009**, *113*, 20594; f) N. P. Wickramaratne, V. S. Perera, B. Park, M. Gao, G. W. McGimpsey, S. D. Huang, M. Jaroniec, *Chem. Mater.* **2013**, *25*, 2803.

[13] a) X. Huang, K. Qian, J. Yang, J. Zhang, L. Li, C. Yu, D. Zhao, *Adv. Mater.* **2012**, *24*, 4419; b) W. Gao, Y. Wan, Y. Dou, D. Zhao, *Adv. Energy Mater.* **2011**, *1*, 115; c) Y. Fang, Y. Lv, R. Che, H. Wu, X. Zhang, D. Gu, G. Zheng, D. Zhao, *J. Am. Chem. Soc.* **2013**, *135*, 1524.

[14] a) J. Park, K. J. An, Y. S. Hwang, J. G. Park, H. J. Noh, J. Y. Kim, J. H. Park, N. M. Hwang, T. Hyeon, *Nat. Mater.* **2004**, *3*, 891; b) C. B. Murray, C. R. Kagan, M. G. Bawendi, *Annu. Rev. Mater. Sci.* **2000**, *30*, 545; c) D. V. Talapin, J.-S. Lee, M. V. Kovalenko, E. V. Shevchenko, *Chem. Rev.* **2010**, *110*, 389.

[15] M. Xu, D. Fujita, K. Sagisaka, E. Watanabe, N. Hanagata, *ACS Nano* **2011**, *5*, 1522.

[16] a) M. A. Worsley, T. T. Pham, A. Yan, S. J. Shin, J. R. I. Lee, M. Bagge-Hansen, W. Mickelson, A. Zettl, *ACS Nano* **2014**, *8*, 11013; b) C. Cui, W. Qian, Y. Yu, C. Kong, B. Yu, L. Xiang, F. Wei, *J. Am. Chem. Soc.* **2014**, *136*, 2256; c) C. Wang, Y. Wang, J. Graser, R. Zhao, F. Gao, M. J. O'Connell, *ACS Nano* **2013**, *7*, 11156; d) A. Reina, X. Jia, J. Ho, D. Nezich, H. Son, V. Bulovic, M. S. Dresselhaus, J. Kong, *Nano Lett.* **2009**, *9*, 30; e) A. C. Ferrari, J. C. Meyer, V. Scardaci, C. Casiraghi, M. Lazzeri, F. Mauri, S. Piscanec, D. Jiang, K. S. Novoselov, S. Roth, A. K. Geim, *Phys. Rev. Lett.* **2006**, *97*, 187401.

[17] Y. Deng, T. Yu, Y. Wan, Y. Shi, Y. Meng, D. Gu, L. Zhang, Y. Huang, C. Liu, X. Wu, D. Zhao, *J. Am. Chem. Soc.* **2007**, *129*, 1690.

[18] a) H. Yang, Y. Yan, Y. Liu, F. Zhang, R. Zhang, Y. Meng, M. Li, S. Xie, B. Tu, D. Zhao, *J. Phys. Chem. B* **2004**, *108*, 17320; b) N. Gokulakrishnan, N. Kania, B. Leger, C. Lancelot, D. Grosso, E. Monflier, A. Ponchel, *Carbon* **2011**, *49*, 1290.

[19] a) L. Chen, Z. Wang, C. He, N. Zhao, C. Shi, E. Liu, J. Li, *ACS Appl. Mater. Interfaces* **2013**, *5*, 9537; b) D. Cai, S. Wang, L. Ding, P. Lian, S. Zhang, F. Peng, H. Wang, *J. Power Sources* **2014**, *254*, 198.

[20] F. Han, Y. Bai, R. Liu, B. Yao, Y. Qi, N. Lun, J. Zhang, *Adv. Energy Mater.* **2011**, *1*, 798.

[21] S. Yang, X. Feng, L. Zhi, Q. Cao, J. Maier, K. Muellen, *Adv. Mater.* **2010**, *22*, 838.

[22] J. Yi, X. P. Li, S. J. Hu, W. S. Li, L. Zhou, M. Q. Xu, J. F. Lei, L. S. Hao, *J. Power Sources* **2011**, *196*, 6670.

[23] G. Li, L. Xu, Q. Hao, M. Wang, Y. Qian, *RSC Adv.* **2012**, *2*, 284.

[24] a) H. Zeng, J. Li, Z. L. Wang, J. P. Liu, S. Sun, *Nano Lett.* **2004**, *4*, 187; b) A. Dong, J. Chen, J. M. V. Patrick, J. M. Kikkawa, C. B. Murray, *Nature* **2010**, *466*, 474.

Received: February 12, 2015
Revised: March 5, 2015
Published online: March 31, 2015

